Development of Flat Panel Active Phased Array Antennas Using 5G Silicon RFICs at *Ku-* and *Ka*-Bands

JIA-CHI SAMUEL CHIEH[1], (Senior Member, IEEE), **EVERLY YEO**[1], **RAIF FARKOUH**[1],
ALEJANDRO CASTRO[1], **MAXWELL KERBER**[1], **RANDALL B. OLSEN**[1],
EMMANUEL J. MERULLA[2], (Member, IEEE), AND
SATISH KUMAR SHARMA[3], (Senior Member, IEEE)

[1]Naval Information Warfare Center Pacific, San Diego, CA 92152, USA
[2]C5ISR Center, United States Army, Aberdeen Proving Ground, MD 21005, USA
[3]Electrical and Computer Engineering Department, San Diego State University, San Diego, CA 92182, USA

Corresponding author: Jia-Chi Samuel Chieh (sam.chieh@navy.mil)

ABSTRACT This article presents the design and development of two all flat panel phased array antennas (PAA) by using emerging 5G Silicon radio frequency integrated circuits (RFICs) at Ku- and Ka-bands. First, an X-/Ku-band wideband dual circular polarized Transmit (Tx)/Receive (Rx) phased array antenna with the capability of scanning ($\pm 45°$) is presented. The frequency of operation is centered around 12.5 GHz within the X/Ku-Bands (3dB Axial Ratio (AR) bandwidth at broadside = 32%). The array has 16-elements with a 4×4 lattice arrangement. This array utilizes a nested sequential rotation architecture, which enhances the axial ratio (AR) bandwidth. Secondly, a dual slant linear polarized ($\pm 45°$) transmit and receive (T/R) phased array antenna, that operates in the Ka-Band and covers the millimeter-wave 5G band (27.5 – 28.35 GHz) is discussed. Beam scanning range is up to $\pm 60°$ in both polarizations. In both cases, the array apertures have been integrated with an active beamforming networks (BFN) utilizing 5G silicon Tx/Rx beamformer RFIC chips. Measured and simulated performance results agree reasonably well in both cases. These arrays are scalable to larger size arrays to provide higher gain for applications like satellite communications (SATCOM) and 5G communications.

INDEX TERMS Silicon RFICs, dual circular polarized, dual slant linear polarized, flat panel phased arrays, SATCOM, 5G communications.

I. INTRODUCTION

Phased array antennas for line of sight communications are preferable as they support agile beam steering. For SATCOM applications, mechanically scanned antennas are viable but suffer from the keyhole effect [1], and the slewing from the gimbal may require a dual antenna solution. The phased array is a preferred solution as the beam can be electronically scanned almost instantaneously so a single antenna aperture can handle the satellite handover. The availability of commercial silicon beamforming chipsets has resulted in the ability for phased array antennas to be ubiquitous in future communication systems. The fully integrated chipset eliminates the

The associate editor coordinating the review of this manuscript and approving it for publication was Ding Xu.

need for discrete transceiver blocks and includes a polarization switch, a transmit/receive (T/R) switch, low noise amplifier, power amplifier, phase shifters, and variable attenuators. The fully integrated chipset reduces overall size, cost, and RF losses.

System level considerations are central to phased array beamforming chipsets, specifically regarding the level of integration. In [2] and [3] the researchers demonstrate high level of integration with a single silicon die beamformer that supports 16-antennas that operates in the W-Band. Alternatively, in [4] researchers present a more discretized solution where the silicon beamformer supports 4-antennas and operates in the Ka-Band. As the frequency of operation lowers, decreasing the level of integration on the silicon chipset can become advantageous. This is largely due to the increase in

inter-elemental spacing in the antenna elements as the frequency decreases. Going to a more discretized array architecture where the silicon chipset has fewer antenna channels has several advantages including lowering the complexity of the silicon chipsets and moving complex routing to the printed circuit board lowering cost, removing single point of error as error is distributed across more antenna elements, allowing for a more scalable architecture, enabling faster design cycles, spreading the heat across the array, and finally improving the yield as the chips are less complex and smaller in size.

In [5] researchers presented a SATCOM Ku-Band phased array antenna, demonstrating dual-linear polarized antennas. This array was developed as a receive only utilizing an 8- channel chipset. In [6] a 28 GHz quad-channel silicon beamformer is used to realize a 64-element T/R array utilizing dual-linear polarized antenna elements. In [7] a 28 GHz quad-channel silicon on insulator (SOI) beamformer chipset is presented covering frequencies from 22 – 44 GHz, the entire millimeter-wave 5G bands.

In this article, we present performance results of the all flat panel phased array antenna (PAAs) designs using commercial 5G Silicon RFICs which do not need an external heatsink. The innovation in the paper is in two parts. First, an X-/Ku-band wideband dual circular polarized transmit (Tx)/receive (Rx) PAA is discussed. There are very few documented circular polarized phased array antennas that utilize active RFIC beamformers, and even fewer with that demonstrates a wide 3-dB axial ratio bandwidth of 32% (broadside), that we present. We present secondly, a dual slant linear polarized Tx/Rx PAA, that operates in the Ka-Band and covers the millimeter-wave 5G band (27.5 – 28.35 GHz). Using this array, we demonstrate over-the-air reception of digitally modulated signals (300 Mbps) up to 30° scan angles. There are few documented papers in literature that demonstrate this. This article highlights the use of RFIC beamformers to design active flat panel phased array antennas rather than conventional phased arrays where discrete RF components are used. Finally we also include brief description of commercial RFICs, important design guidelines, printed circuit board (PCB) layout, fabrication and other challenges in designing such arrays.

II. COMMERCIAL SILICON RFIC BEAMFORMERS

The emerging 5G silicon RFICs benefits in an extremely low profile phased array antenna design. The fully integrated chipset eliminates the need for discrete transceiver blocks. The fully integrated chipset reduces overall size, cost, and RF losses. Several commercial chipsets are now widely available operating in the Ku- and Ka- bands. Table 1 shows a sampling between several commercial silicon beamforming chipsets, showing frequencies of operation, number of channels, and T/R functionality. One of the commercial RFICs used for our Ka-Band design is the Anokiwave AWMF-0116 chipset. Fig. 1 shows a systems level schematic of the integrated beamformer. This single-channel chipset operates from 26 – 30 GHz, and incorporates a RF switch, to shift

TABLE 1. Limited sampling of Commercial Silicon Beamforming Chipsets.

Ref	Vendor	Model	Freq. (GHz)	# Channels	T/R
[8]	Analog Devices	ADMV4821	24–29.5	16	Tx/Rx
[9]	Analog Devices	ADMV4801	24-29.5	16	Tx/Rx
[10]	Analog Devices	ADAR1000	8-16	8	Tx/Rx
[11]	Renesas	F5268	24.2-27.5	8	Tx/Rx
[12]	Renesas	F6502	27-31	8	Tx
[13]	Renesas	F6503	14-16	8	Tx
[14]	Renesas	F6123	14.4-17.3	16	Rx
[15]	Anokiwave	AWMF-0117	10.5-16	1	Tx/Rx
[16]	Anokiwave	AWMF-0151	26.5-29.5	4	Tx/Rx
[17]	Mixcomm	SUMMIT2629	26.5-29.5	8	Tx/Rx
[18]	RF Core	RMF120160PA	12-16	4	Tx/Rx
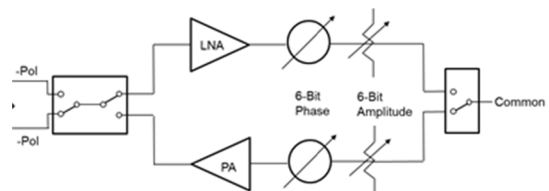
FIGURE 1. System level schematic of silicon beamformer chipset from Anokiwave AWMF-0116/0117.

between transmit and receive paths, as well as switching between two polarizations. Both transmit and receive paths offer 6-bit of amplitude and phase control, with a noise figure (NF) of 5 dB and an output P1dB of 12 dBm. The chipset is single-channel and comes in a flip-chip package. The size of the chipset is 2.5 mm x 2.5mm. The chip consumes 220 mW on receive and 370 mW on transmit.

Similarly, the commercial beamformer chipset for the Ku-band PAA design used was the Anokiwave AWMF-0117, which shares the same system level schematic shown in Fig. 1. This chipset is a single-channel T/R chip that can support dual polarizations and operates between 10.5 – 16 GHz. On transmit channel has 20 dB of gain with an OP1dB of 12 dBm. On receive channel there is 28 dB of gain with a Noise Figure of 3 dB and an input third order intercept point (IIP3) of -19 dBm. On transmit it has a 1 dB compression point output power (OP1dB) of +12 dBm. Both transmit and receive paths have 6-bit control over both amplitude/attenuator. The chipset also has 6-bit phase shifters (average RMS phase error of 5°). This chipset uses double pull double throw (DPDT) switch to support dual-polarizations. The chip comes in a wafer level chip scale (WLCS) flip-chip package. The chip consumes 200 mW on receive and 250 mW on transmit.

III. MULTILAYER PCB STACKUP CONSIDERATIONS

Multilayer PCBs are necessary for realizing all flat panel PAAs. In [19] researchers developed a phased array utilizing a silicon RFIC with an organic substrate, liquid crystal polymer (LCP) for a low cost higher performance solution. In [20] researchers integrated a silicon beamformer with an
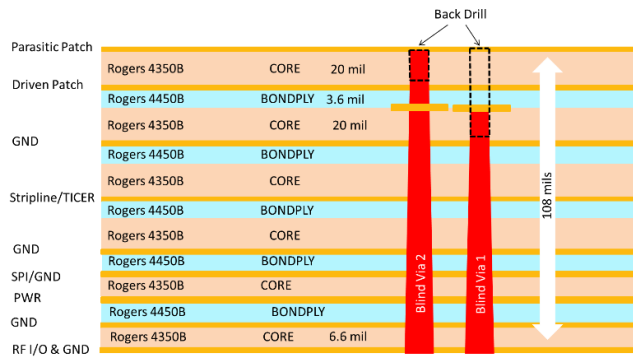
FIGURE 2. Proposed Multi-layer PCB Stackup.

FIGURE 3. Cross-section of PCM showing blind vias.

antenna array developed on low-temperature co-fired ceramic (LTCC). In [21]–[23] researchers utilized printed circuit board laminates to integrate the silicon beamformer with antenna array for a low cost, high yield, high performance solution. We have adopted a similar approach. Fig. 2 shows the PCB stackup used for the Ku-band array. Rogers 4350 (ε_r = 3.48 and tan δ = 0.004) is used throughout the board. The total thickness of the PCB is 108 mils. Inter-layer thicknesses are not shown due to proprietary nature of the design. The stacked patch elements reside on two 20 mil layers. The feed distribution layer resides on stripline utilizing Wilkinson power combiners. This feed distribution layer also utilizes embedded NiCr foil resistors from Ticer^{TM}. Various power, ground, and digital routing planes reside underneath the stripline feed layer to provide biasing and control to the chipsets. Finally, finite ground plane co-planar waveguide (FGCPW) are used to route RF signal from the chip to the antennas and from the chip to the corporate feed network. Two blind vias are used in this design. The first is used to route RF signal to the driven patch element. The second is used to stitch ground vias around the stripline feed network. These blind vias are back-drilled, filled with dielectric hole material, and then cap-plated. Back-drilling allows for a single copper plating cycle, resulting in finer tolerances and feature sizes on the printed circuit board (PCB). Fig. 3 shows a photograph cut cross-section of a part of a process control monitor (PCM) structure that shows connection of the two blind vias. A small residual stub is a by-product of back drilling. If the residual stub is too great, it can act as an open stub resonator. Similar is the board stackup description for Ka-band array hence is not repeated again. The main difference is that the antennas reside on two 10 mil layers, reducing the antenna substrate height for higher frequency operation. Intermediate layers remain the same.

A. PCB LAYOUT CONSIDERATIONS

Since the phase array antennas reside on multi-layer laminated dielectric materials, several layout considerations are made. Fig. 4 shows a picture from Altium (PCB software) with the stripline metal layer (in yellow) and bottom metal layer (in blue) turned on. The printed circuit board has 10 metal layers with an internal stripline layer for the feed
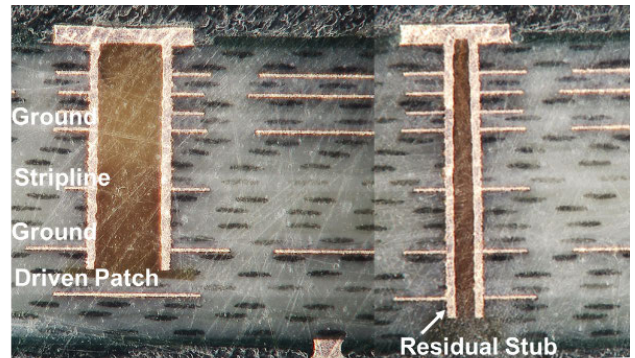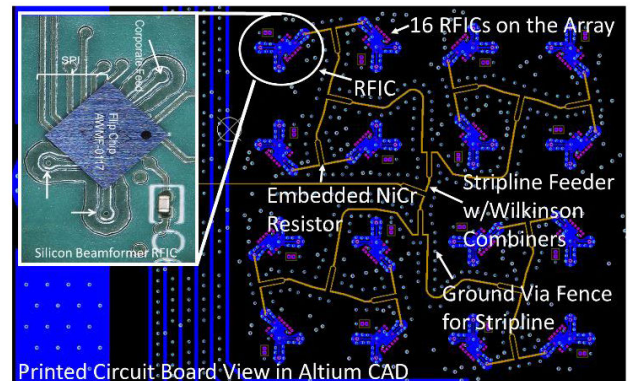

FIGURE 4. View of the Stripline Feeder in Altium CAD software for PCB design. View shows in blue (bottom metal layer), yellow (inner stripline layer). Inset picture shows flip-chip mounting of the beamformer RFIC.

distribution. Via fence surrounds the stripline transmission line. Inset into Fig. 4 shows a physical picture of the RFIC mounted to the printed circuit board. This also includes SPI controller for applying beam forming algorithms. Minimum trace width and spacing of 5mils are maintained throughout the design. Minimum via diameters of 8mils are used.

IV. KU-BAND DUAL CIRCULAR POLARIZED PHASED ARRAY ANTENNA

Circular polarized active electronically scanned arrays (AESAs) are of great interest for satellite communications (SATCOM). Phased arrays which are capable of maintaining circular polarization (CP) over wide scan angles are of great interest especially for new satellite constellation that are being deployed in Low-Earth Orbit (LEO) and Medium-Earth Orbit (MEO). LEO constellations are closer to earth ($\sim$500-2000 km) and therefore move overhead at a much faster rate and require fast hand-off from horizon to horizon. Several efforts have been made in the past to develop low profile CP phased array antennas. In [24] an X-band dual polarized CP phased array was developed for submarine SATCOM using complex multi-chip-modules (MCM) on low-temperature co-fired ceramic (LTCC) material. The performance of the axial-ratio (AR) bandwidth over scan

angles was not presented. In [25], a wide-scan linear phased array antenna was presented with AR < 3dB beamwidth of 121° with co- to cross-polarization separation of 16 dB. This array however utilizes Magnetic-Electric dipoles as the radiators, and therefore has a narrow impedance bandwidth (2%). In [26] and [27] a truncated corner patch phased array was realized, however demonstrated narrow axial bandwidths of 2.4% and 3.2% respectively at broadside. In [28] a dual-linear patch antenna array was coupled with a beamformer RFIC, which combined the two linear polarizations on-chip with a 90° offset to generate the circular polarization. This method yielded a 6.7% AR bandwidth at broadside, however AR properties over the scan angles and frequency was not included.

One method that has been used to enhance the AR bandwidth in passive fixed beam arrays is to use sequential rotation (SQR) and nested SQR [29]–[32]. In nested SQR approach, radiator elements within a sub-array utilize SQR, and then SQR is applied at the sub-array level. All of these examples are variations of using sequential rotation to realize a passive fixed broadside beam array. This section presents an active wide AR bandwidth dual-circular polarized Tx/Rx phased array antenna (PAA) which is implemented utilizing nested SQR. The antenna aperture has been integrated with beamforming network using 5G Silicon RFICs and multi-layer PCBs as discussed in the earlier section.

A. SINGLE ELEMENT DESIGN

In order to support dual circular polarizations with a wide impedance bandwidth, several radiator topologies could be adopted as described in [33]. A well-known corner truncated probe fed stacked patch approach was utilized for the phased array design. Fig. 5 shows the dimensions of the stacked patch elements as well as an exploded view of the board stackup used for the phased array. The driven patch is 23.6 mils above the ground plane, and the parasitic patch is 20 mils above the driven patch. A stripline feeder is realized beneath the antenna elements, with a total height of 30 mils. Ticer NiCr foil resistors are implemented on this stripline layer for the 3dB Wilkinson power splitters. Wilkinson splitters/combiners are used in place of T-Junctions in order to mitigate likelihood of the array oscillating. The total thickness of the PCB is 108 mils. Rogers 4350B ($\varepsilon_r = 3.66$, tan $\delta = 0.002$) is used as the dielectric substrate. The antenna is fed through a via, which is back-drilled to disconnect it from the parasitic patch.

Fig. 6(a) shows the simulated reflection coefficient magnitude of the radiating element. It can be observed that an impedance bandwidth ($S_{11} = -10$dB criteria) from $12 - 14.5$ GHz can be obtained. Fig. 6(b) shows the simulated gain radiation pattern for both left hand circular polarization (LHCP) and right hand circular polarization (RHCP) at design frequency, $f_o = 12.5$ GHz, with a peak gain of 3 dBi and a 3dB beamwidth of 104°. The co- to cross- polarization separation is better than 20dB. Fig. 7(a) shows the AR for broadside pattern over frequency. As can be seen, the AR bandwidth is fairly narrow at 3% centered

Rogers 4350B $\varepsilon_r = 3.66$, tan $\delta = 0.002$
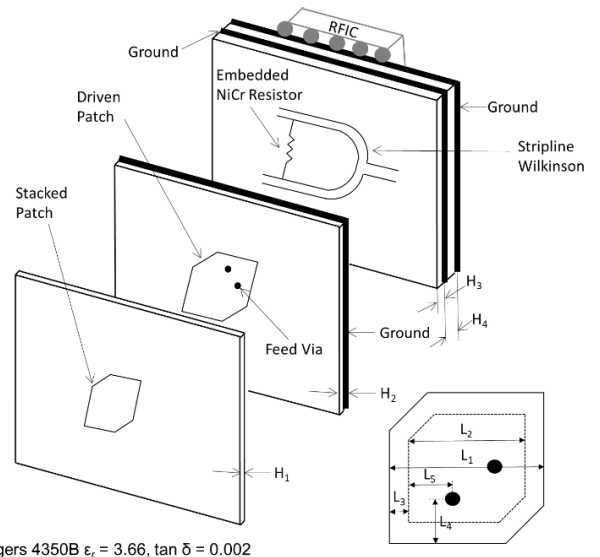
FIGURE 5. Truncated corner stacked patch antenna element. Antenna parameters are: $H_1 = 0.508$mm, $H_2 = 0.599$mm, $H_3 = 0.975$mm, $H_4 = 0.127$mm, $L_1 = 5.79$mm, $L_2 = 5.41$mm, $L_3 = 0.187$mm, $L_4 = 0.61$mm, $L_5 = 2.69$mm.
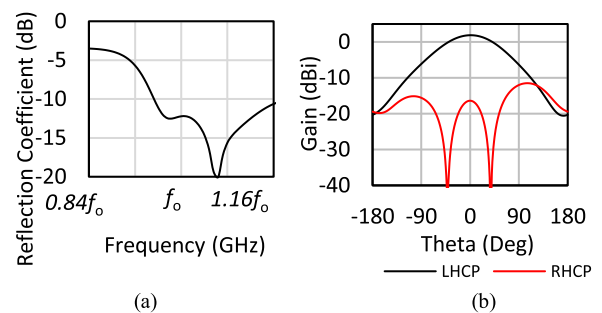
FIGURE 6. Simulated (a) reflection coefficient, and (b) gain pattern at 12.5 GHz, where f_o is 12.5 GHz.
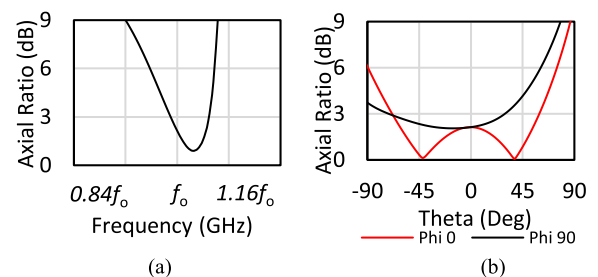
FIGURE 7. Simulated (a) AR vs. frequency, and (b) AR beamwidth, where f_o is 12.5 GHz.

at 12.5 GHz. Fig. 7(b) shows the AR beamwidth for both $\varphi = 0°$ and $\varphi = 90°$ cut planes at the design frequency, and as can be seen, there is little asymmetry. The results from a single polarization (LHCP) is presented for brevity. Since the antenna is symmetric, the performance and characteristics of the other polarization (RHCP) are identical.

B. ANTENNA ARRAY ARCHITECTURE STUDY

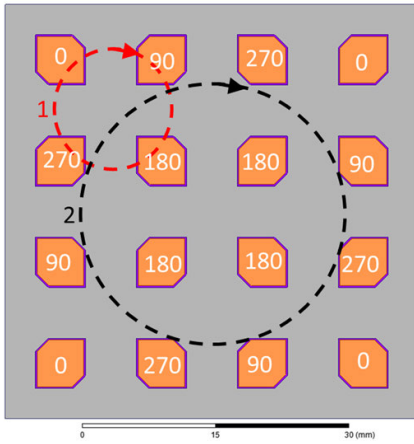Fig. 8 shows nested sequential rotation (SQR) approach based design where both local (#1) and nested SQR (#2) at the

FIGURE 8. Array architectures showing nested sequential rotation (SQR).

sub-array level is applied. The inter-elemental spacing is $0.5\lambda_o$ at the design frequency. The array antenna shares the same PCB stack-up as in Fig. 2 and Fig. 5. In [10], [11] it is shown that the nested SQR improved the AR bandwidth for passive fixed beam arrays. Typically, for passive arrays, a 90° delay transmission line is added to compensate for the sequential rotation. Since our phased array is a fully active antenna, the compensation for the sequential rotation is performed within the RFIC phase shifter, and therefore the delay is frequency dependent. Fig. 9(a-c) shows the simulated AR beamwidth for $\varphi = 0°$ and $\varphi = 90°$ cut planes at f_o for the fixed beam case, AR (dB) versus frequency for the azimuth scan and AR (dB) versus frequency for the elevation scan, respectively.

As can be seen that for the fixed beam case at center frequency, f_o, (Fig. 9(a)), where both local (#1) and nested SQR (#2) is used, the AR beamwidth is symmetric and wide (approximately 50° for $\varphi = 0°$ and $\varphi = 90°$) due to the symmetry in the array orientation. Fig. 9(b) and (c) shows the results when the proposed nested SQR is used for scan angles in the Azimuth and Elevation planes, respectively. The 3dB AR fractional bandwidth for Azimuth and Elevation scan angles up to 45° beam scan is 28% and 16%, respectively. As can be seen, the AR is flat over frequency and over scan angles. Here, positive beam scan angles are shown for LHCP case for brevity, which remains the same for RHCP and for the negative beam scan angles. As the scan angle increase, the progressive phase shift also increases, disrupting the phase continuity of the sequential rotation. In all cases, the appropriate phase compensation due to the sequential rotation is introduced through a phase shifter.

C. PROTOTYPE CP DUAL-POLARIZED PHASED ARRAY

A 16-element 4 × 4 phased array antenna using the nested SQR concept was designed and fabricated. Fig. 10 shows the photograph of the fabricated prototype which includes multilayer PCB and Altium layout considerations Anokiwave AWMF-0117 single channel silicon beamforming RFICs
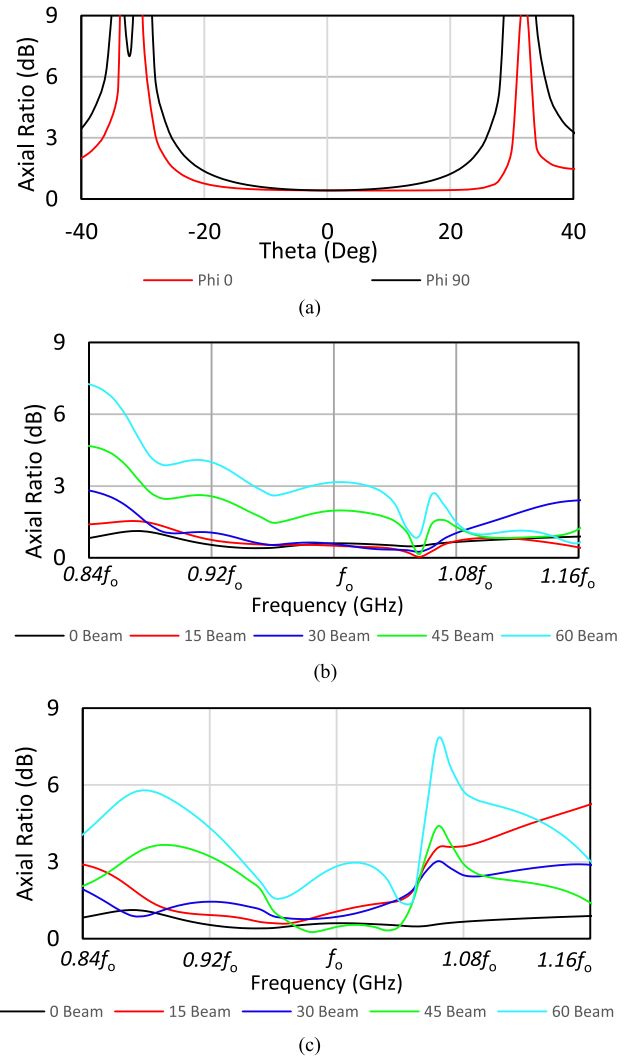

(a)

(b)

(c)

FIGURE 9. Simulated axial ratio (AR) for the nested sequential rotation based array (Fig. 8) for (a) fixed beam case at f_o: AR (dB) versus elevation angle, (b) Azimuth scan case: AR (dB) versus frequency, and (c) Elevation scan case: AR (dB) versus frequency. Here f_o is 12.5 GHz.
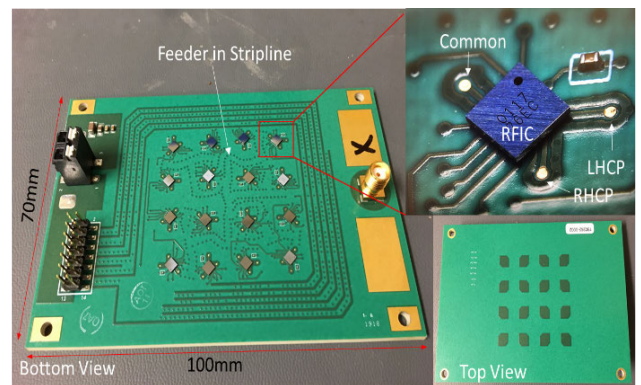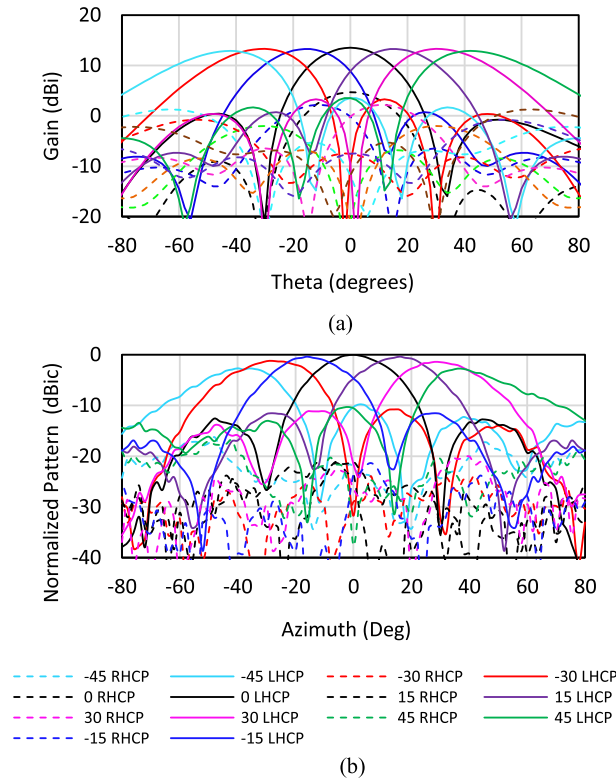

FIGURE 10. Photograph of the fabricated prototype phased array antenna.

were used. Phase compensation due to the nested sequential rotation is applied using this chipset. Beamforming algorithm was applied through SPI controller and Labview based
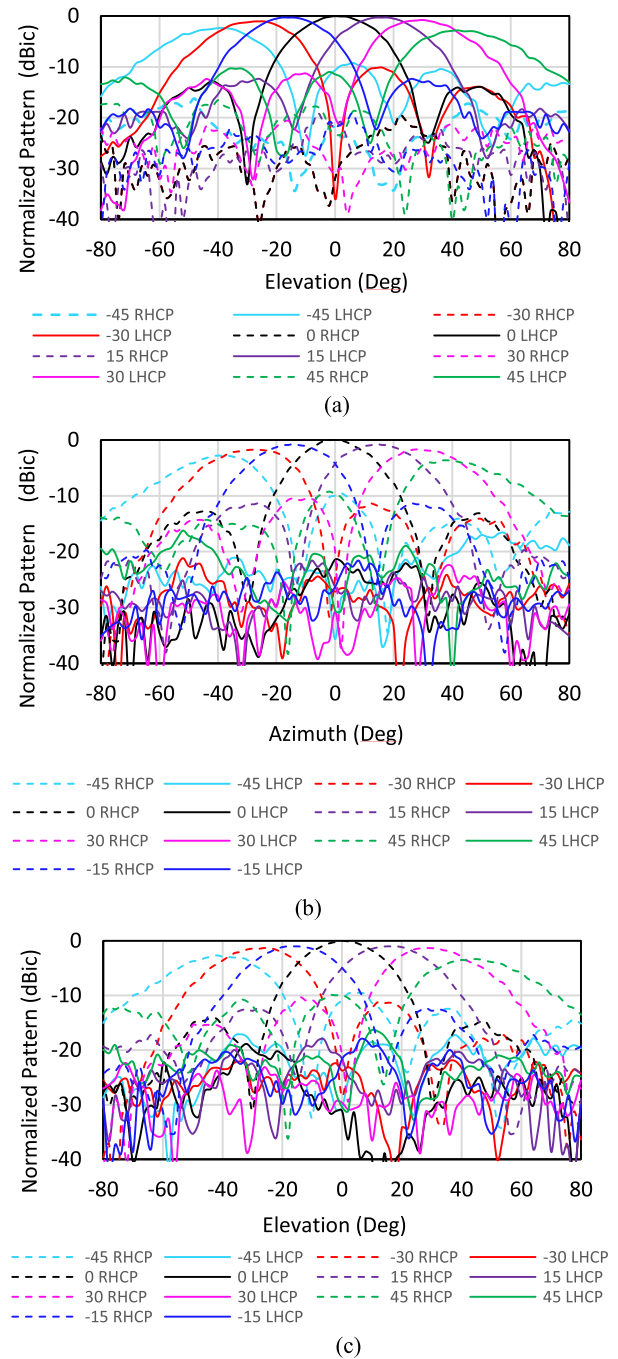
FIGURE 11. (a) Simulated LHCP beam scan patterns for Azimuth at 12.5 GHz, and (b) measured LHCP beam scan patterns for Azimuth at 12.5 GHz.

graphical user interface (GUI) which controls beam peak scan angles. Radiation pattern measurements were performed at San Diego State University's far-field anechoic chamber. The presented measured beam patterns are normalized since this array has gain on receive in addition to the feed network losses. Similarly, S-parameter is the combined effect of the active and passive components so not included here. Fig. 11 shows the simulated and measured azimuth (x-z plane) beam scan patterns for the LHCP polarization at $f_o = 12.5$ GHz and they correlate very well. Measurements were performed up to $\pm 80°$ due to constraints on the test setup in the anechoic chamber. The measured difference between the LHCP and RCHP over frequency and scan angle is approximately better than 20 dB.

Fig. 12(a) shows the measured normalized elevation (y-z plane) scanned patterns for the LHCP polarization. Fig. 12(b) shows the measured normalized azimuth scanned patterns for the RHCP polarization. Fig.12(c) shows the measured normalized elevation scanned patterns for the RHCP polarization. The chipset allows for support of dual-polarization through a DPDT T/R switch. When switching between the LHCP and RHCP, since nested SQR is used, the phase compensation applied through the phase shifter is reversed. The beam scanned patterns for both azimuth and elevation scans in both LHCP and RHCP polarizations match very well.

Fig. 13 shows the measured axial ratio (AR) versus frequency for both polarizations (LHCP and RHCP) and for the

FIGURE 12. (a) Measured LHCP beam scan patterns for Elevation at 12.5 GHz, (b) Measured RHCP beam scan patterns for Azimuth at 12.5 GHz, and (c) Measured RHCP beam scan patterns for Elevation at 12.5 GHz.

axial ratio bandwidth when the beam is scanned away from the broadside both elevation and azimuth cut planes, and can be compared with Figs. 9(b-c) simulated AR results for these cases. The measured 3dB AR bandwidth for scan angles up to $\pm 30°$ is 24% for both cut-planes. For both LHCP and RHCP polarizations on azimuth cut plane, the axial ratio is remains below 3 dB for scan angles up to $\pm 45°$. However, for both LHCP and RHCP in the elevation cut plane, the axial ratio for $+45°$ and $-45°$ are degraded to around 6-7dB, corresponding

TABLE 2. Comparison Table of CP active phased arrays.

Reference	Frequency Band	Array Topology	Polarization	3dB AR Bandwidth Broadside	3dB AR 30° Beam Scan Bandwidth	Array Size
[23]	Ku-Band	Linear	V/H Linear	N/A	N/A	8x8
[24]	X-Band	Non SQR	RHCP/LHCP	--	--	4x18
[25]	C-Band	ME-Dipole	RHCP/LHCP	<2%	--	1x8
[26]	S-Band	Non SQR	RHCP/LHCP	2.4%	2.4%	1x8
[27]	Ka-Band	Non SQR	RHCP/LHCP	3.2%	0.8%	1x8
[28]	Ka-Band	Combined Linear	RHCP/LHCP	6.7%	--	16x16
This Work	X/Ku-Band	Nested SQR	RHCP/LHCP	32%	24%	4x4

with expected simulated results, which can still be usable for some communication applications.

Table 2 shows a comparison of circular polarized active phased arrays in literature, where the beamformers are fully integrated. This works shows significant improvement in the axial ratio bandwidth when the beam is scanned away from the broadside.

V. KA-BAND DUAL SLANT LINEAR POLARIZED PHASED ARRAY ANTENNA

Fifth generation (5G) cellular technology has great potential to address challenges for wireless providers. Millimeter-wave regime has many benefits which include, increased radio frequency (RF) channel bandwidths, lower latency, and ability to exploit spatial processing techniques such as beamforming [34]. Frequency allocation for one of the millimeter-wave 5G bands is at 28 GHz (27.5 – 28.35 GHz) [35]. Notional architectures will include massive multiple input multiple output (MIMO) [14] and/or hybrid approaches, which will incorporate RF beamforming as discussed by [36]– [40].

In this section, we present a 64-element T/R array with dual slant linear ($\pm45°$) polarized elements utilizing emerging 5G silicon RFICs which offer the benefit of an extremely low profile design (4 mm thick). Slant polarization resulted in a more optimized board layout due to lattice spacing limitations. At the same time, slant polarization is often used in cellular base station antennas [41] to improve propagation under different fading environments. It is also well known that slant polarized elements are able to receive vertical, horizontal, and circularly-polarized signals. The developed 64-element T/R array that operates from 26 –30 GHz. Comparison between simulation and measurement results are presented. This work was presented in part in [42], and this article expands with new material utilizing this array for over the air (OTA) testing.

A. RADIATING ELEMENT DESIGN

To match the broad operating bandwidth of the chipset, stacked patch elements were used [44], [45]. The parasitic square microstrip patch has a width of 2.3 mm and the driven square microstrip patch has a width of 2.2 mm. The patch elements are separated by a 0.254 mm Rogers 4350 substrate and are probe fed with two 0.2 mm vias for dual polarization. The radiating element is impedance matched ($S_{11} = -10$ dB) from 25 – 31 GHz, however is not shown because the novelty is in the implementation of the phased array rather than the radiating element used.

B. PLANAR ARRAY DESIGN

The lattice spacing of the array is 6.6 mm, which is equal to 0.62λ at 28 GHz, where λ is the free space wavelength. The elements are oriented at $\pm45°$ to offer dual slant polarization. This spacing and orientation was chosen as a balance between antenna array performance and accommodation of the placement of the silicon beamforming chips on the backside of the board. The lattice inter-element spacing has been chosen considering the grating lobe free scan volume. During the design phase, mutual coupling was minimized considering the selected inter-element spacing. However, if one wants to reduce mutual coupling further, it can be achieved by increasing spacing between the radiating elements. Also, techniques such as metamaterial baffle in-between antenna elements or ground via rings around the antenna can reduce mutual coupling further. In the presented PAA designs, since mutual coupling was acceptable for the most part hence we did not choose to add a mutual coupling reduction technique. Further, the complexity of the beamforming board precluded us from applying these techniques. Simulations of the array were completed in Ansys high frequency structure simulator (HFSS) using the domain decomposition method (DDM) as shown in Fig. 14. Measurement of active phased array efficiency is tedious and can only be obtained through high fidelity calibration. Losses and gains from the whole RF chain would need to be measured and characterized including the RFIC, the RFIC to PCB board transition, stripline feeder, and transitions from RFIC to antenna. These losses/gains cannot be measured directly and would require dedicated calibration structures in order to de-embed the radiation efficiency, hence has not been performed here. The simulated radiation efficiency of the phased array antenna is 66%, 70%, 78%, and 82% at 26 GHz, 27 GHz, 28 GHz, and 29 GHz, respectively.
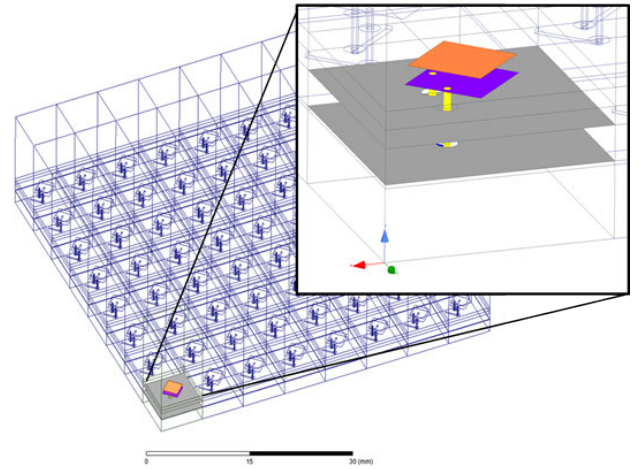
Legend:
- -45deg_AR
- -30deg_AR
- +0deg_AR
- +15deg_AR
- +30deg_AR
- +45deg_AR
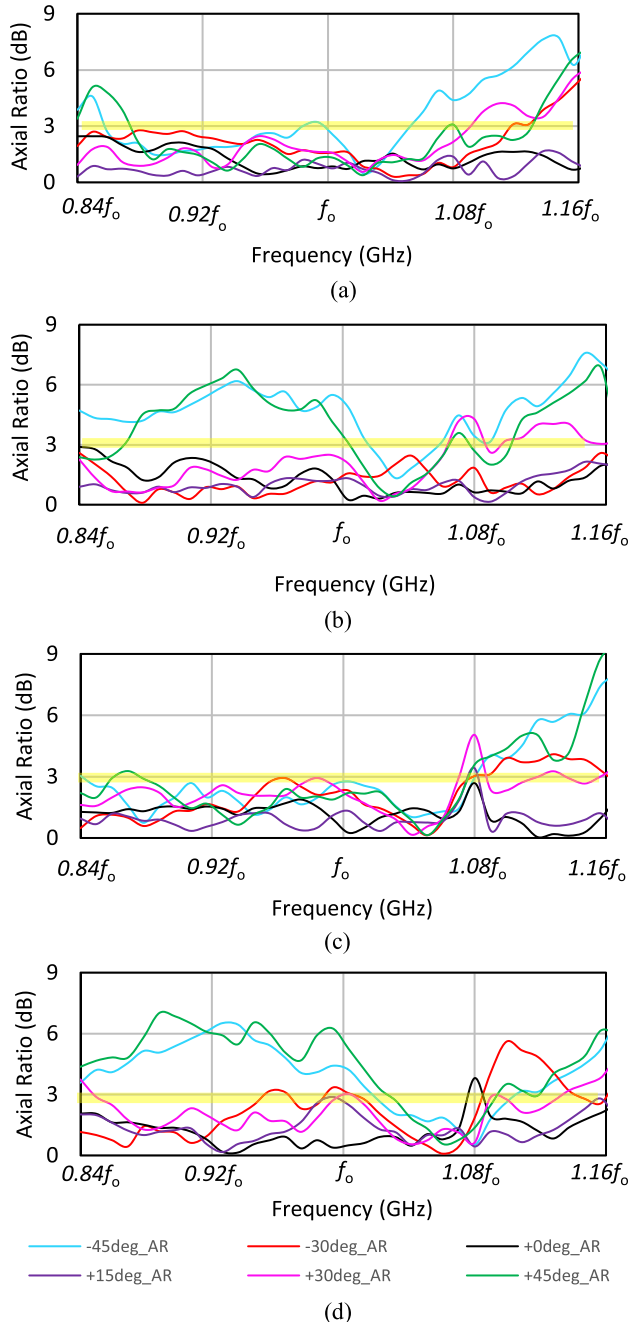
FIGURE 13. (a) LHCP AR Azimuth scan, (b) LHCP AR Elevation scan, (c) RHCP AR Azimuth scan, (c) RHCP AR Elevation scan. Here f_O is 12.5 GHz.

FIGURE 14. Ansys HFSS DDM simulation model showing single radiating element cell which employs stacked patches.

FIGURE 15. Developed 64-Element T/R phased array at 28 GHz.

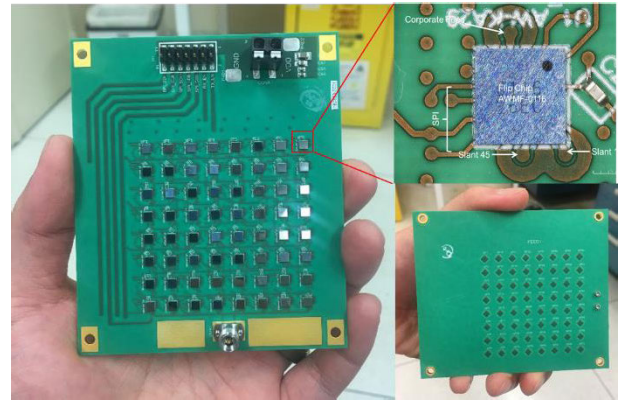**FIGURE 16.** Phased array under test in anechoic chamber.

C. PROTOTYPE DUAL SLANT LINEAR POLARIZED ARRAY

The developed phased array is shown in Fig. 15. Fig. 16 shows the antenna array under test at the Antenna and Microwave Lab (AML) at San Diego State University. The phased array antenna utilizes a vertical mount 2.92 mm coaxial connector for RF input and output. A custom LabVIEW user interface was developed to control the array via SPI. This software allows for beam scanning in both planes as well as the application of various amplitude tapers.
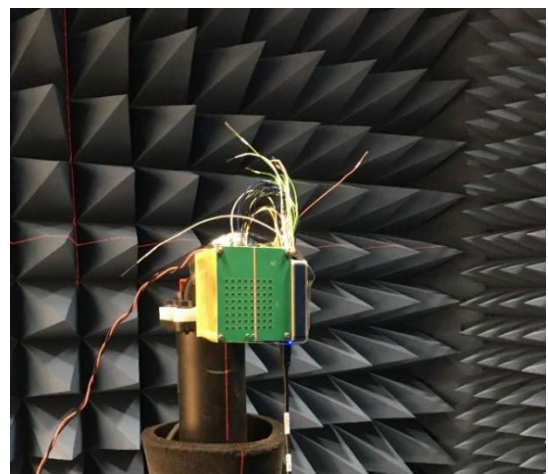
The 3D printed mount we used in the chamber had a small offset, so all measurements also reflect this same offset.

Fig. 17 shows the simulated and measured normalized array beam scan patterns for azimuth scanning under uniform excitation when selected linear polarization is $\phi = 45°$ at 28 GHz. As can be seen, the simulated and measured results correspond very well with the beam scanning up to $\pm 55°$ with
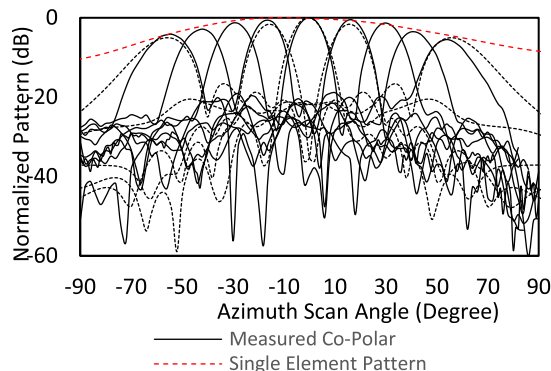
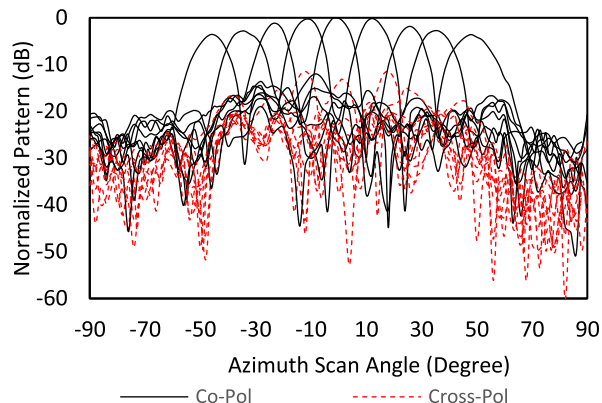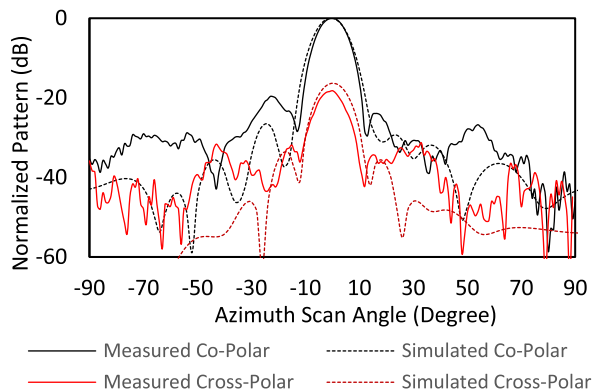**FIGURE 17.** Simulation and Measurement of Azimuth Scan at 45°-Pol, 28 GHz.

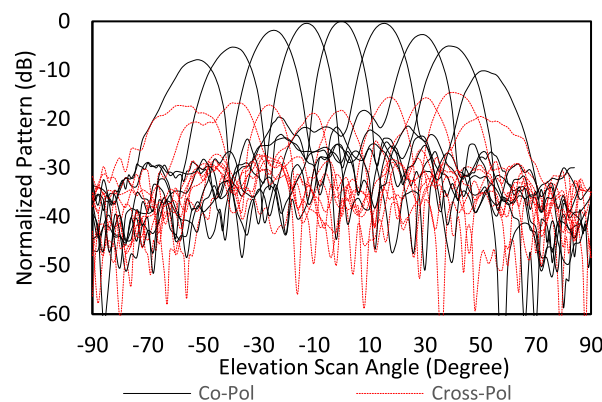**FIGURE 18.** Simulation and Measurement of Broadside Co- and Cross-Polar patterns at 28 GHz.

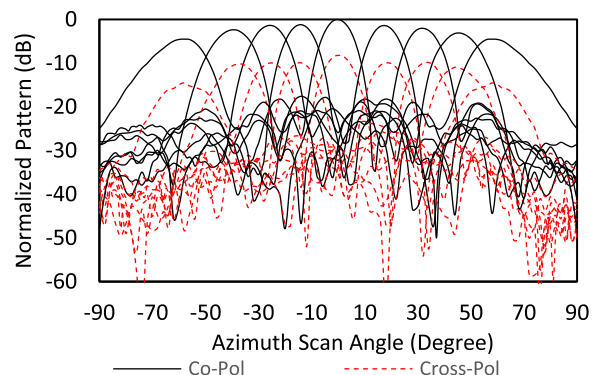**FIGURE 19.** Measurement of Azimuth Scan at 45°-Pol, 26 GHz.

FIGURE 20. Measurement of Azimuth Scan at 45°-Pol, 30 GHz.

FIGURE 21. Measurement of Vertical Scan at -45°-Pol, 28 GHz.
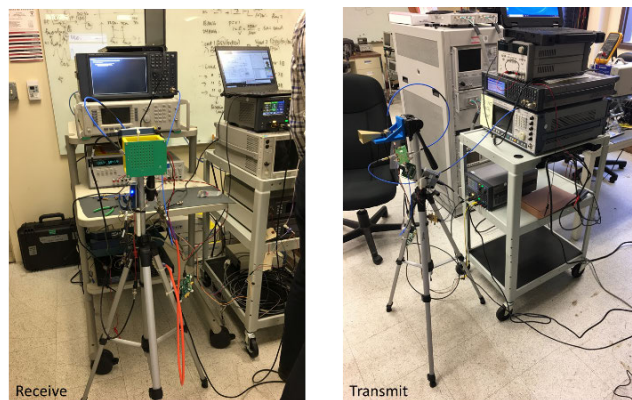

FIGURE 22. Over-the-air (OTA) testing set-up.

a 5 dB drop from broadside. As can be seen, the array patterns follow the pattern envelope of the single antenna element. Fig. 18 shows the measured and simulated co-polarization and cross-polarization patterns at 28 GHz, and as can be seen correlate fairly well. Similarly, Fig. 19 and 20 shows the measured beam scan patterns at 26 GHz and 30 GHz respectively for the $\phi = 45°$ linear polarization. In measurement the phase weights were calculated at 26 GHz, and these weights were kept the same for all other frequencies. Since the inter-elemental spacing is fixed, and the phase weights are static, as the frequency increases, the scan angle becomes reduced. In theory, the phase weights could be re-calculated

at each frequency to ensure the scan angle performance. Measured cross- polarization levels are at least 10 dB below the main lobe. and $\phi = 90°$ are the array planes. Fig. 21 shows measurement results for elevation scanning when $\phi = -45°$ or 135° at 28 GHz. Sidelobe levels are less than 20 dB from the main lobe as measurements were taken in the $\phi = 45°$ cut plane, while $\phi = 0°$. The gain roll-off in this plane is more severe with a 7.8 dB drop when the beam is scanned to $\pm 55°$. The reason for this is that the beamwidth of the single

TABLE 3. Comparison of Ka-Band active phased array antennas.

Reference	Frequency Band	Polarization	Link Distance	RFIC Channels	Integration Approach	Array Size
[27]	Ka-Band	Linear	--	--	Antenna in PCB	1x8
[45]	Ka-Band	Dual Linear	50m	16	Antenna in Package	8x8
[46]	Ka-Band	Dual Linear	--	16	Antenna in Package	2x4
[48]	Ka-Band	Dual Linear	300m	4	Antenna in PCB	8x8
[48]	Ka-Band	Dual Linear	2.5m	24	Antenna in Package	4x6
This Work	Ka-Band	Dual Slant Linear	20m	1	Antenna in PCB	8x8
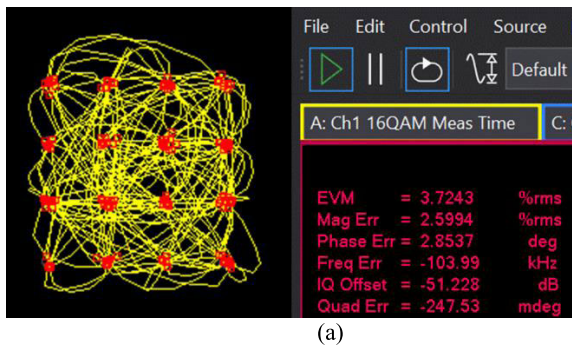
(a)
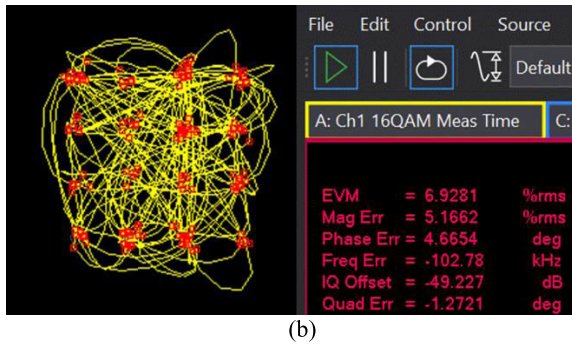
(b)

FIGURE 23. Constellation at (a) broadside and (b) +30° with 16-QAM.

FIGURE 24. Constellation at broadside with 64-QAM.

D. OVER THE AIR (OTA) TESTING

Finally, over the air (OTA) tests (Fig. 22) with digitally modulated signals were performed in our laboratory. On transmit, a Keysight N5172B signal generator was used to provide the digitally modulated signal. The signal generator provided an intermediate frequency (IF) of 1.8 GHz, which was up converted to 28 GHz with the Anokiwave AWMF- 0170 Ka-Band active mixer integrated circuit (IC). A standard gain horn (15 dBi) was used as the transmit antenna. On receive, the developed Ka-Band phased array antenna was used. Another AWMF-0170 converter IC was used to down-convert the 28 GHz signal back to 1.8 GHz. A Keysight E4440A
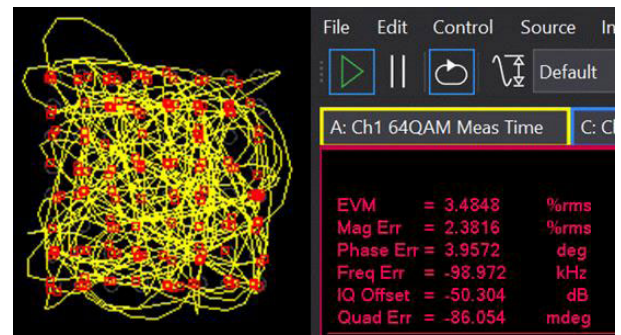
spectrum analyzer was used to receive the digitally modulated signal. Finally, Keysight 89600 VSA software was used to demodulate the signal and recover the constellation. The transmit and receive antennas were placed approximately 20m apart from each other. Initially 16-QAM with a signal bandwidth of 75 Msps was used to test the link (300 Mbps). This data rate is representative of potential radios that might be used with this phased array antenna. Fig. 23(a) shows the recovered constellation using a broadside beam and Fig. 23(b) shows the recovered constellation using a +30° beam. The RMS error vector magnitude (EVM) of the recovered signal is 3.7% and 6.9% respectively. Fig. 24 shows a recovered constellation of a broadside beam using a higher order modulation, using 64-QAM with a signal bandwidth of 10 Msps (60 Mbps), showing an RMS EVM of 3.48%.

Finally, Table 3 shows a comparison of other active phased array antennas developed using silicon beamforming chipsets and operating in the Ka-Band. Our work represents the only design realized with dual-slant linear polarization, while using an antenna in PCB integration approach, and using single-channel silicon beamforming core chipsets.

VI. CONCLUSION

We have shown in this article two flat panel active phased array antennas that utilize state-of-the-art silicon beamforming RFICs. The first PAA presented is dual-circular polarized operating within the X/Ku-Bands. This array has a wide AR bandwidth over frequency and scan angles (±30°).

The second PAA presented is dual-slant linear polarized and we have demonstrated a 20m OTA link up to 300 Mbps with scan angles up to 30°.

ACKNOWLEDGMENT

The authors would like to thank G. Mishra for help in measurement at the Antenna and Microwave Laboratory (AML), San Diego State University. The authors would also like to thank Logan Minard from Anokiwave for valuable discussions.

REFERENCES

[1] R. Gilmore, "Broadband-on-the-move satellites takes the pole position," *MilsatMagazine*, May 2013. [Online]. Available: http://www.milsatmagazine.com/story.php?number=1466984736

[2] A. Natarajan, S. K. Reynolds, M.-D. Tsai, S. T. Nicolson, J.-H. Conan Zhan, D. Gun Kam, D. Liu, Y.-L. Oscar Huang, A. Valdes-Garcia, and B. A. Floyd, "A fully-integrated 16-element phased-array receiver in SiGe BiCMOS for 60-GHz communications," *IEEE J. Solid-State Circuits*, vol. 46, no. 5, pp. 1059–1075, May 2011.

[3] S. Shahramian, M. J. Holyoak, and Y. Baeyens, "A 16-element W-band phased-array transceiver chipset with flip-chip PCB integrated antennas for multi-gigabit wireless data links," *IEEE Trans. Microw. Theory Techn.*, vol. 66, no. 7, pp. 3389–3402, Jul. 2018.

[4] K. Kibaroglu, M. Sayginer, and G. M. Rebeiz, "A low-cost scalable 32-element 28-GHz phased array transceiver for 5G communication links based on a 2 × 2 beamformer flip-chip unit cell," *IEEE J. Solid-State Circuits*, vol. 53, no. 5, pp. 1260–1274, May 2018.

[5] A. H. Aljuhani, T. Kanar, S. Zihir, and G. M. Rebeiz, "A scalable dual-polarized 256-element ku-band phased-array SATCOM receiver with ±70° beam scanning," in *IEEE MTT-S Int. Microw. Symp. Dig.*, Jun. 2018, pp. 1203–1206.

[6] K. Kibaroglu, M. Sayginer, T. Phelps, and G. M. Rebeiz, "A 64-element 28-GHz phased-array transceiver with 52-dBm EIRP and 8–12-Gb/s 5G link at 300 meters without any calibration," *IEEE Trans. Microw. Theory Techn.*, vol. 66, no. 12, pp. 5796–5811, Dec. 2018.

[7] L. Gao and G. M. Rebeiz, "A 22-44-GHz phased-array receive beamformer in 45-nm CMOS SOI for 5G applications with 3-3.6-dB NF," *IEEE Trans. Microw. Theory Techn.*, early access, Jul. 3, 2020, doi: 10.1109/TMTT.2020.3004820.

[8] *ADMV4821 Data Sheet*, ADMV4821, Analog Devices, Norwood, MA, USA, 2020.

[9] *ADMV4801 Data Sheet*, ADMV4821, Analog Devices, Norwood, MA, USA, 2020.

[10] *8 GHz to 16 GHz, 4-Channel, X Band and Ku Band Beamformer*, ADAR1000, Analog Devices, Norwood, MA, USA, 2020.

[11] *Transmit/Receive Half Duplex IC 24.25 GHz to 27.5 GHz*, F5268, Renesas, Tokyo, Japan, May 2020.

[12] *Ka-Band SATCOM Transmitter IC 27 GHz to 31 GHz*, F6502, Renesas, Tokyo, Japan, Sep. 2018.

[13] *Common Data Link (CDL) Tx IC 14 GHz to 16 GHz*, F6503, Renesas, Tokyo, Japan, Sep. 2018

[14] *16-Channel Dual-Beam Rx Active Beamformer IC, Ku/CDL Band*, F6123, Renesas, Tokyo, Japan, May 2020

[15] *Intelligent Gain Block Ku-Band Silicon IC*, AWMF-0117, Anokiwave, San Diego, CA, USA, 2017

[16] *28 Ghz Silicon 5G Tx/Rx Quad Core Dual-Pol IC*, AWMF-0151, Anokiwave, San Diego, CA, USA, Dec. 2018

[17] *26.5-29.5 GHz TRX Front End IC for 5G TDD mm-Wave*, SUMMIT 2629, Mixcomm, Chatham, NJ, USA, Jun. 2020

[18] *RMF120160PA Core Chip*, document RMF120160PA, RF Core, 2018.

[19] X. Gu, D. Liu, C. Baks, O. Tageman, B. Sadhu, J. Hallin, L. Rexberg, P. Parida, Y. Kwark, and A. Valdes-Garcia, "Development, implementation, and characterization of a 64-element dual-polarized phased-array antenna module for 28-GHz high-speed data communications," *IEEE Trans. Microw. Theory Techn.*, vol. 67, no. 7, pp. 2975–2984, Jul. 2019.

[20] D. G. Kam, D. Liu, A. Natarajan, S. Reynolds, H.-C. Chen, and B. A. Floyd, "LTCC packages with embedded phased-array antennas for 60 GHz communications," *IEEE Microw. Wireless Compon. Lett.*, vol. 21, no. 3, pp. 142–144, Mar. 2011.

[21] A. Nafe, M. Sayginer, K. Kibaroglu, and G. M. Rebeiz, "2 × 64-element dual-polarized dual-beam single-aperture 28-GHz phased array with 2 × 30 Gb/s links for 5G polarization MIMO," *IEEE Trans. Microw. Theory Techn.*, vol. 68, no. 9, pp. 3872–3884, Sep. 2020.

[22] Y. Yin, S. Zihir, T. Kanar, Q. Ma, H. Chung, L. Gao, and G. M. Rebeiz, "A 37-42-GHz 8×8 phased-array with 48-51-dBm EIRP, 64-QAM 30-Gb/s data rates, and EVM analysis versus channel RMS errors," *IEEE Trans. Microw. Theory Techn.*, early access, Jun. 8, 2020, doi: 10.1109/TMTT.2020.2998183.

[23] A. H. Aljuhani, E. Traffenstedt, T. Kanar, S. Zihir, and G. M. Rebeiz, "Ultra-low cost ku-band dual-polarized transmit and receive phased-arrays for SATCOM and point-to-point applications with bandwidths up to 750 MHz," in *Proc. IEEE Int. Symp. Phased Array Syst. Technol. (PAST)*, Oct. 2019, pp. 8138–8143.

[24] K. M. Lee, J. Edie, R. Krueger, J. Weber, T. Brott, and W. Craig, "A low profile X-band active phased array for submarine satellite communications," in *Proc. IEEE Int. Conf. Phased Array Syst. Technol.*, May 2000, pp. 231–234.

[25] Y.-Q. Wen, B.-Z. Wang, and X. Ding, "Wide-beam circularly polarized microstrip magnetic-electric dipole antenna for wide-angle scanning phased array," *IEEE Antennas Wireless Propag. Lett.*, vol. 16, pp. 428–431, 2017.

[26] P. Liu, Y. Li, and Z. Zhang, "Circularly polarized 2 bit reconfigurable beam-steering antenna array," *IEEE Trans. Antennas Propag.*, vol. 68, no. 3, pp. 2416–2421, Mar. 2020.

[27] T. Lambard, O. Lafond, M. Himdi, H. Jeuland, S. Bolioli, and L. Le Coq, "Ka-band phased array antenna for high-data-rate SATCOM," *IEEE Antennas Wireless Propag. Lett.*, vol. 11, pp. 256–259, 2012.

[28] K. K. Wei Low, A. Nafe, S. Zihir, T. Kanar, and G. M. Rebeiz, "A scalable circularly-polarized 256-element ka-band phased-array transmitter with ±60° beam scanning and 34.5 dBW EIRP," in *IEEE MTT-S Int. Microw. Symp. Dig.*, Jun. 2019, pp. 1064–1067.

[29] P. S. Hall, "Application of sequential feeding to wide bandwidth, circularly polarised microstrip patch arrays," *IEE Proc. H-Microw., Antennas Propag.*, vol. 136, no. 5, pp. 390–398, Oct. 1989.

[30] T. Teshirogi, M. Tanaka, and W. Chujo, "Wideband circularly polarised array antennas with sequential rotations phase shift of elements," in *Proc. Int. Symp. Antennas Propag.*, ISAP, Tokyo, Apr. 1985, pp. 117–120.

[31] R. R. George, A. T. Castro, and S. K. Sharma, "Comparison of a four stage sequentially rotated wideband circularly polarized high gain microstrip patch array antennas at ku-band," in *Proc. 11th Eur. Conf. Antennas Propag. (EUCAP)*, Mar. 2017, pp. 2307–2311.

[32] A. Chen, Y. Zhang, Z. Chen, and C. Yang, "Development of a *Ka*-band wideband circularly polarized 64-element microstrip antenna array with double application of the sequential rotation feeding technique," *IEEE Antennas Wireless Propag. Lett.*, vol. 10, pp. 1270–1273, 2011.

[33] P. Sharma and K. Gupta, "Analysis and optimized design of single feed circularly polarized microstrip antennas," *IEEE Trans. Antennas Propag.*, vol. AP-31, no. 6, pp. 949–955, Nov. 1983.

[34] T. S. Rappaport, S. Sun, R. Mayzus, H. Zhao, Y. Azar, K. Wang, G. N. Wong, J. K. Schulz, M. Samimi, and F. Gutierrez, "Millimeter wave mobile communications for 5G cellular: It will work," *IEEE Access*, vol. 1, pp. 335–349, 2013.

[35] W. Roh, J.-Y. Seol, J. Park, B. Lee, J. Lee, Y. Kim, J. Cho, K. Cheun, and F. Aryanfar, "Millimeter-wave beamforming as an enabling technology for 5G cellular communications: Theoretical feasibility and prototype results," *IEEE Commun. Mag.*, vol. 52, no. 2, pp. 106–113, Feb. 2014.

[36] M. V. Komandla, G. Mishra, and S. K. Sharma, "Investigations on dual slant polarized cavity-backed massive MIMO antenna panel with beamforming," *IEEE Trans. Antennas Propag.*, vol. 65, no. 12, pp. 6794–6799, Dec. 2017.

[37] K. Kibaroglu, M. Sayginer, A. Nafe, and G. M. Rebeiz, "A dual-polarized dual-beam 28 GHz beamformer chip demonstrating a 24 gbps 64-QAM 2×2 MIMO link," in *Proc. IEEE Radio Freq. Integr. Circuits Symp. (RFIC)*, Jun. 2018, pp. 64–67.

[38] R. Garg and A. S. Natarajan, "A 28-GHz low-power phased-array receiver front-end with 360° RTPS phase shift range," *IEEE Trans. Microw. Theory Techn.*, vol. 65, no. 11, pp. 4703–4714, Nov. 2017.

[39] U. Kodak and G. M. Rebeiz, "A 5G 28-GHz common-leg T/R front-end in 45-nm CMOS SOI with 3.7-dB NF and −30-dBc EVM with 64-QAM/500-MBaud modulation," *IEEE Trans. Microw. Theory Techn.*, vol. 67, no. 1, pp. 318–331, Jan. 2019.

[40] B. Yu, K. Yang, C.-Y.-D. Sim, and G. Yang, "A novel 28 GHz beam steering array for 5G mobile device with metallic casing application," *IEEE Trans. Antennas Propag.*, vol. 66, no. 1, pp. 462–466, Jan. 2018.

[41] R. Valkonen, "Compact 28-GHz phased array antenna for 5G access," in *IEEE MTT-S Int. Microw. Symp. Dig.*, Jun. 2018, pp. 1334–1337.

[42] B. Yang, Z. Yu, J. Lan, R. Zhang, J. Zhou, and W. Hong, "Digital beamforming-based massive MIMO transceiver for 5G millimeter-wave communications," *IEEE Trans. Microw. Theory Techn.*, vol. 66, no. 7, pp. 3403–3418, Jul. 2018.

[43] J.-C.-S. Chieh, E. Yeo, M. Kerber, R. Olsen, E. Merulla, and S. Sharma, "A 28 GHz dual slant polarized phased array using silicon beamforming chipsets," in *Proc. IEEE Int. Symp. Phased Array Syst. Technol. (PAST)*, Oct. 2019, pp. 1–5.

[44] R. B. Waterhouse, "Design of probe-fed stacked patches," *IEEE Trans. Antennas Propag.*, vol. 47, no. 12, pp. 1780–1784, Dec. 1999.

[45] M. A. Matin, B. S. Sharif, and C. C. Tsimenidis, "Probe fed stacked patch antenna for wideband applications," *IEEE Trans. Antennas Propag.*, vol. 55, no. 8, pp. 2385–2388, Aug. 2007.

[46] H.-T. Kim, B.-S. Park, S.-S. Song, T.-S. Moon, S.-H. Kim, J.-M. Kim, J.-Y. Chang, and Y.-C. Ho, "A 28 GHz CMOS direct conversion transceiver with packaged antenna arrays for 5G cellular system," in *Proc. IEEE Radio Freq. Integr. Circuits Symp. (RFIC)*, Jun. 2017, pp. 69–72.

[47] K. Kibaroglu, M. Sayginer, and G. M. Rebeiz, "A scalable 64-element 28 ghz phased-array transceiver with 50 dbm eirp and 8-12 gbps 5g link at 300 meters without any calibration," in *IEEE MTT-S Int. Microw. Symp. Dig.*, Jun. 2018, pp. 496–498.

[48] J. D. Dunworth, A. Homayoun, B.-H. Ku, Y.-C. Ou, K. Chakraborty, G. Liu, T. Segoria, J. Lerdworatawee, J. W. Park, H.-C. Park, H. Hedayati, D. Lu, P. Monat, K. Douglas, and V. Aparin, "A 28GHz bulk-CMOS dual-polarization phased-array transceiver with 24 channels for 5G user and basestation equipment," in *IEEE ISSCC Dig. Tech. Papers*, Feb. 2018, pp. 70–72.

JIA-CHI SAMUEL CHIEH (Senior Member, IEEE) received the B.S. degree in electrical engineering from the University of California at San Diego, La Jolla, CA, USA, in 2004, the M.S. degree in electrical engineering from the University of Southern California, Los Angeles, CA, USA, in 2007, and the Ph.D. degree in electrical engineering from the University of California at Davis, Davis, CA, USA, in 2012. He was a Student Intern at PlanarMag Inc., in the summer of 2009, aiding in the development and design of magnetic baluns for TV set-top boxes. In the summer of 2010, he was a Student Intern with LGS Innovations (formerly Bell Laboratories), Florham Park, NJ, USA, aiding in the development and modeling of millimeter-wave antennas, arrays, and flip-chip packages. In 2012, he joined the Naval Information Warfare Center Pacific (NIWC-PAC), San Diego, where he is currently the RF Lead for the Integrated Circuits Technology Branch. Since 2013, he has been serving as an Adjunct Lecturer with the University of San Diego. Since 2018, he has been serving as an Adjunct Faculty with San Diego State University. His current research interests include developing microwave and millimeter-wave phased arrays for directional networking as well as novel antennas for nanosatellite applications. He has designed over six RFIC-based phased array antennas from C- through *W*-bands. He has been the Principle Investigator of three ONR funded S&T projects at the 6.2 level.

EVERLY YEO received the B.S. and M.Eng. degrees in electrical engineering from the University of California at San Diego, in 2005 and 2006, respectively. He joined the Naval Information Warfare Center Pacific (NIWC-PAC), San Diego, in 2006. His research interests include analog, RF, and mixed-signal integrated circuit design and hardware systems. His work experience and interests include silicon CMOS chip-level design of auto-zeroing comparators, bandgap references, automatic gain control circuits, and test chip vehicles for process characterization. He has been involved in advanced testing of millimeter-wave 10-GB/s *E*-band radios for ship-to-shore applications. He has also worked on hardware designs of several *Ku*-, *Ka*-, and *X*-bands active steerable antenna arrays, high-power distribution boards for unmanned systems, and transceiver communication systems.
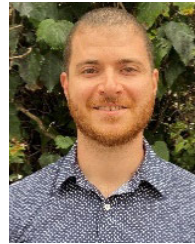
RAIF FARKOUH received the B.S. and M.S. degrees in electrical engineering from the University of Nebraska, Lincoln, in 2017. His specialty was microelectronics. He has worked as an Electrical Engineering Intern at Nebraska Public Power District, where he has worked on the design and specification of power and control systems, system layouts, load calculations, and equipment sizing and selection. He has worked as an Electrical Engineering Intern with Jensen Hughes consulting company, where he performed circuit analysis and supporting tasks to support safe-shutdown analysis of a nuclear power station. He also worked as a Research Assistant with the University of Nebraska, where he developed and carried out research projects to demonstrate capability of Femtosecond laser machining. In 2018, he joined the Naval Information Warfare Center Pacific (NIWC-PAC), San Diego, CA, as an Electrical Engineer. He is the Primary Investigator for a project with the goal to develop wideband low-cost electronically scanned *Ka*-band circular polarized antenna array technology to provide DoD ground and space-based systems with electronically steerable high-level system arrays capable of supporting LEO small satellite constellations. He has designed several phased array antennas in the *X*-, *Ku*-, and *Ka*-bands. He also supported the testing and evaluation of novel RF Integrated Circuits, including amplifiers, filters, and antenna array chipsets.

ALEJANDRO CASTRO received the B.S. and M.S. degrees in electrical engineering from San Diego State University (SDSU), in 2015 and 2017, respectively. His thesis topic was "Novel Antenna Designs Using 3D Printing and Inkjet Printing Technologies." He was a Student Intern at Taoglas, from 2015 to 2016. In summer 2016, he was a Student Intern for the DOD Naval Research Enterprise Internship Program (NREIP). He helped to design a *W*-band reflector horn antenna for Cube Satellite application. In 2017, he was a RF Engineer at Space Micro Inc. At Space Micro, he was a Co-PI (a Private Investigator) on two different SBIR Phase I contracts for the MDA and NAVAIR. In 2019, he joined the Naval Information Warfare Center Pacific (NIWC Pacific), as a New Professional, where he joined the Applied Electromagnetics Branch. He is currently working on millimeter-wave electronically scanned phase array antenna and supporting various applications. He also supports testing and tuning of HF antennas.

MAXWELL KERBER received the B.S. degree in physics and the Master of Engineering (M.E.) degree in electrical engineering from the University of California at San Diego, San Diego, in 2006 and 2007, respectively. Since 2008, he has been a part of the Advanced Integrated Circuit Technology Branch, Naval Information Warfare Center Pacific (NIWC-PAC). His research interests include low-power radio frequency (RF) energy harvesting, near field wireless power transfer, and phased array antenna command and control. He has developed control interfaces for several generations of phased array antennas developed at NIWC-PAC.

RANDALL B. OLSEN received the B.A. degree in mathematics and the B.S. degree *(summa cum laude)* in physics from the University of California at Riverside, in 1974, and the Ph.D. degree in physics from Princeton University, in 1979. He was a Postdoctoral Fellow in physics with the University of California at San Diego. He has served as the President and the CTO of Chronos Research Laboratories, Inc., San Diego, CA. He founded Chronos to develop a solid-state, heat-to-electrical energy conversion technology. He was the Principal Investigator on 17 SBIR Phase I contracts and four Phase II contracts with NASA, DOE, SDIO, AFOSR, ARO, DNA, and others. He served as the Group Manager/General Manager–Broadband Wireless at ThermoTrex Corporation/Trex Enterprises Corporation, San Diego. He co-invented over 15 broadband wireless devices and systems and installed the world's first 1.25-Gb/s wireless data link that operates at more than 70 GHz. He was a Co-Inventor of ThermoTrex's second-generation Millimeter Wave Imager (94 GHz) and its Dielectric Slab Antenna and Program Manager for NASA AITP Millimeter-Wave Passive Ultra-Compact Imaging Technology for Synthetic Vision and Mobile Platforms (210 GHz). He was the Principal Investigator on a DARPA study to design a large aperture millimeter-wave imager (78–96 GHz). He served as the Director of RF Systems at AirFiber, San Diego, CA, where he developed low-cost, high-performance millimeter wave radios for gigabit-capable fixed wireless communication systems at 70–80 GHz (1.25 Gb/s) for mass production. In 2003, he joined what is now called the Naval Information Warfare Center Pacific, San Diego, as the Scientist. He is currently developing networking technology which uses low-cost electronically-steered directional antennas for high-data rate ad hoc communications. He invented the concepts for, and served as PI on, SPAWN (including 3 at-sea experiments in Trident Warriors) for OPNAV, BEAMS (brassboard hardware) for ONR, and Directional Ad hoc Networking TEchnology (DANTE) for SSC-Pacific. He also serves as the Chief Engineer on a JCTD [Mobile Unmanned/Manned Distributed Lethality Airborne Network (MUDLAN)]. He won the SSC-Pacific's Galileo Award as the center's top creative scientist, in 2007. He received the Dr. Delores M. Etter Top Navy Scientist and the Engineer of the Year Award, in July 2011.

EMMANUEL J. MERULLA (Member, IEEE) received the B.S. and M.S. degrees in electrical engineering from the University of Connecticut, Storrs, CT, USA, in 2006 and 2008, respectively. He started his technical training as a Radar/IFF Technician for the U.S. Navy, from 1994 to 2001. After finishing with the Navy, he returned to the University of Connecticut, to study antenna engineering, where he worked for National Science Foundation studying wireless power transfer in waveguides. In 2005, he interned for MegaWave Corporation, where he started building wideband baluns for an Army application as well as an automatic antenna measuring system for the company. In 2006, he joined MegaWave, full time, where he designed numerous antennas anywhere from low-frequency applications to millimeter wave applications. He was the Principle Investigator on a millimeter wave program, where he developed an on body wireless personal area network that operated in the 60-GHz band that incorporated wireless power systems. In 2014, he joined the C5ISR Center, as a Senior Modeling and Simulation Engineer. His primary duty was the simulation and placement of antenna system to coexist on the same military platform. Since 2016, he became the millimeter-wave Product Lead under the Non Traditional Waveforms program and the Government Team Lead.

SATISH KUMAR SHARMA (Senior Member, IEEE) received the B.Tech. degree from the Kamla Nehru Institute of Technology, in 1991, and the Ph.D. degree from IIT, Banaras Hindu University (BHU), in 1997, all in electronics engineering. From March 1999 to April 2001, he was a Postdoctoral Fellow with the Department of Electrical and Computer Engineering, University of Manitoba, MB, Canada. He was a Senior Antenna Engineer with InfoMagnetics Technologies Corporation, Winnipeg, MB, Canada, from May 2001 to August 2006. He was also a Research Associate with the University of Manitoba, from June 2001 to August 2006. In August 2006, he joined San Diego State University (SDSU), San Diego, as an Assistant Professor with the Department of Electrical and Computer Engineering. Here, he has developed the Antenna Laboratory, teaches courses in applied electromagnetics, and advises B.S., M.S., and Ph.D. students; and Postdoctoral Fellows. Since 2014, he has been a Full Professor and the Director of the Antenna and Microwave Laboratory (AML). He is author/coauthor of more than 285 research articles published in the referenced international journals and conferences. He has co-edited three volumes of the *Handbook of Reflector Antennas and Feed Systems*, *Theory and Design of Reflectors* (Volume I), *Feed Systems* (Volume II), and *Applications of Reflectors* (Volume III) (Artech House, USA). He holds one U.S. and one Canadian patents. His main research interests include the millimeter wave antennas, beam steering antennas, massive MIMO antennas, 5G communication antennas, beamforming networks, antennas for the IoT, microstrip antennas, ultra-wideband, multiband and broadband antennas, reconfigurable and frequency agile antennas, feeds for reflector antennas, waveguide horns and polarizers, electrically small antennas, RFID antennas, active antennas, frequency selective surfaces, metasurfaces, and microwave passive components. He received the IEEE AP-S Harold A. Wheeler Prize Paper Award in 2015, the National Science Foundation's Prestigious Faculty Early Development (CAREER) Award in 2009, and the Young Scientist Award of URSI Commission B, Field and Waves, during the URSI Triennial International Symposium on Electromagnetic Theory, Pisa, Italy, in 2004. He was recognized as the Outstanding Associate Editor (AE) for the IEEE Transactions on Antennas and Propagation (IEEE TAP) journal in July 2014. He has served as the AE for the IEEE TAP, and currently serving as the AE for the IEEE Antennas and Wireless Propagation Letters. He was the Chair/Co-Chair of the several Student Paper Contests in different conferences and symposia and served on the sub-committee of the Education Committee for the IEEE Antennas and Propagation Society for the organization of the Student Paper Contests. He is a full member of the USNC/URSI, Commission B, Fields and Waves, and also serving as the Chair, Technical Activities for the same.

• • •